1 **Impact of deoxygenation and hydrological changes on the Black Sea nitrogen cycle during**

2 **the Last Deglaciation and Holocene**

4 Anna Cutmore[1*]., Nicole Bale[1]., Rick Hennekam[2]., Bingjie Yang[1]., Darci Rush[1]., Gert-Jan Reichart[2,3]., Ellen C.

5 Hopmans[2]., Stefan Schouten[1,3]

7 [1]*Department of Marine Microbiology & Biogeochemistry, NIOZ Royal Netherlands Institute for Sea Research, 1790 AB Den Burg,*

8 *Netherlands*

9 [2]*Department of Ocean Systems, NIOZ Royal Netherlands Institute for Sea Research, 1790 AB Den Burg, Netherlands*

10 [3]*Department of Earth Sciences, Universiteit Utrecht, Princetonlaan 8a, 3584 CB Utrecht, Netherlands*

11 *Corresponding Author: anna.cutmore@nioz.nl

13 **Abstract**

14 The marine nitrogen (N) cycle profoundly impacts global ocean productivity. Amid rising deoxygenation in

15 marine environments due to anthropogenic pressures, understanding the impact of this on the marine N-cycle

16 is vital. The Black Sea's evolution from an oxygenated lacustrine basin to an anoxic marine environment over

17 the last deglaciation and Holocene offers insight into these dynamics. Here, we generated records of the organic

18 biomarkers heterocyte glycolipids, crenarchaeol, and bacteriohopanetetrol, associated with various water-

19 column microbial N-cycle processes, which indicate a profound change in Black Sea N-cycle dynamics at ~7.2 ka

20 when waters became severely deoxygenated. This transition substantially reduced Thaumarchaeota-driven

21 nitrification and enhanced loss of bioavailable nitrogen through anaerobic ammonium oxidation (anammox). In

22 contrast, other climatic changes over the last deglaciation and Holocene, such as freshwater input, water-level

23 variations and temperature changes, did not impact these processes. Cyanobacterial nitrogen fixation in surface

24 waters proved more responsive to changes in salinity which affected species composition, and associated water

25 column stratification which reduced vertical transport of nutrients. Our results indicate that future

26 deoxygenation in certain marine environments may enhance bioavailable nitrogen loss by anammox and reduce

27 nitrification by Thaumarchaeota, while enhanced stratification may increase cyanobacterial nitrogen fixation in

28 the surface waters.

29

30 **1. Introduction**

31 The marine nitrogen (N) cycle is a significant control of biological productivity in the global oceans. It is directly

32 connected to the fixation of atmospheric carbon dioxide and carbon export from the ocean's surface, influencing

33 atmospheric CO_2 levels over geological time scales (Falkowski et al., 1998). As the marine N-cycle is strongly

34 regulated by biology, the (de)oxygenation of the ocean determines the microorganisms involved in these

35 biogeochemical cycles and the aerobic/anaerobic pathways that occur. Under anoxic conditions, loss of

36 bioavailable nitrogen is substantial, attributed to anaerobic ammonium oxidation (anammox) and denitrification

37 (Kuypers et al., 2003; Dalsgaard et al., 2012). With deoxygenation in marine environments increasing due to

38 anthropogenic climate and environmental changes (i.e., Keeling et al., 2010; Bopp et al., 2013), and research

39 linking deoxygenation to changes in the marine N-cycle (Kalvelage et al., 2013; Naafs et al., 2019), it is important

40   to enhance our understanding of how the marine N-cycle may respond to future deoxygenation and what the

41   associated feedbacks on carbon fixation might be.

42

43   Marine basins that have experienced changes in oxygenation in the past can provide perspective on the current

44   deoxygenation of modern global oceans and the associated feedbacks in the marine N-cycle, in particular on

45   timescales beyond the observational record. Today, the Black Sea is the world's largest permanently stratified

46   anoxic basin with limited connection to the global ocean through the Bosporus Strait and its redox gradient is a

47   hotspot of diverse microbial populations and metabolisms, experiencing many of the same crucial microbial

48   biogeochemical cycle processes as the global ocean (Kusch et al., 2022). However, over the last deglaciation and

49   Holocene (approximately the last 20 ka), the Black Sea experienced large hydrological changes. The basin was

50   an oxygenated fresh-water lacustrine environment during the Last Glacial Maximum (LGM) (Schrader, 1979) and

51   experienced many environmental changes during the subsequent deglaciation, including temperature changes

52   (Bahr et al., 2005; 2008; Ion et al., 2022), water-level variations (Ivanova et al., 2007; Nicholas et al., 2011; Piper

53   & Calvert, 2011), and changes in freshwater input into the basin, both through melting of Eurasian icesheets and

54   alpine glaciers after the LGM and changes in regional precipitation (Bahr et al., 2005; 2006; 2008; Badertscher

55   et al., 2011; Shumilovskikh et al., 2012). It became reconnected to the global ocean at ~9.6 ka when post-glacial

56   sea-level rise caused an initial marine inflow (IMI) over the Bosporus sill (Aksu et al., 2002; Major et al., 2006;

57   Bahr et al., 2008; Ankindinova et al., 2019), leading to enhanced salinity of the water column (Marret et al.,

58   2009; Verleye et al., 2009; Filipova-Marinova et al., 2013) and euxinic deep waters developing in the basin after

59   ~7.2 ka (Arthur & Dean, 1998; Eckert et al., 2013). Thus, sedimentary records of the Black Sea may provide a

60   unique perspective of the impact of deoxygenation, as well as changing temperature and salinity, on the marine

61   N-cycle.

62

63   Diagnostic lipid biomarkers of microbes preserved in the geological record can offer a unique insight into past

64   changes in the N-cycle (Rush & Sinninghe Damsté, 2017 and references cited therein; Elling et al., 2021; van

65   Kemenade et al., 2023), although the limitations of extrapolating modern findings to ancient climates must be

66   acknowledged, as past ecosystems may have operated under different dynamics that are not fully captured by

67   contemporary analogues. Nitrogen fixing heterocytous cyanobacteria play a crucial role in transforming nitrogen

68   gas (N_2) to bioavailable nitrogen (NH_3) and sustaining primary productivity in both marine and freshwater

69   environments (Villareal, 1992; Ploug et al., 2008). Identification of their diagnostic biomarkers, heterocyte

70   glycolipids (HGs), in the geological record are a widely-used proxy for exploring past changes in nitrogen fixation

71   by these microbes (Bauersachs et al., 2009; 2010; Sollai et al., 2017; Bale et al., 2019; Elling et al., 2021; Pérez

72   Gallego et al., 2025). The structure of the sugar moiety of HGs is a useful indicator of paleoenvironmental

73   conditions, as HGs with a hexose (C_6) headgroup are typically found in free-living heterocystous cyanobacteria

74   (Bauersachs et al, 2009; Wörmer et al., 2012), while HGs with a pentose (C_5) headgroup are associated with

75   endosymbiotic heterocystous cyanobacteria in marine diatoms (diatom-diazotroph associations, DDAs)

76   (Schouten et al., 2013; Bale et al., 2015). Consequently, both hexose and pentose HGs have been applied as

77   specific paleo-biomarkers for the presence of N_2-fixing cyanobacteria in marine and lacustrine geological records

(Bauersachs et al., 2010; Sollai et al., 2017; Bale et al., 2019; Elling et al., 2021). Nitrification, the microbial two-step conversion of ammonia (NH_3) and/or ammonium (NH_4^+) to nitrate (NO_3^-), is a central part of the marine N-cycle. Archaea of the phylum Thaumarchaeota (also known as Nitrososphaerota) are among the most abundant and widespread marine prokaryotes (Karner et al., 2001; Francis et al., 2005), playing a crucial role in nitrification in the Black Sea (Lam et al., 2007) by aerobically oxidizing ammonia to nitrite (Könneke et al., 2005; Wuchter et al., 2006). As Thaumarchaeota are the exclusive producers of the membrane spanning lipid, crenarchaeol (Sinninghe Damste et al., 2002), this biomarker can be used to identify Thaumarchaeota in the geological record and explore the paleo marine N-cycle. Another critical part of the N-cycle is the loss of bioavailable nitrogen to N_2. Under anoxic conditions, bioavailable nitrogen (NO_3^-, NO_3^-, NH_3 and NH_4^+) can be lost through two processes in subsurface waters: anammox (van de Graaf et al., 1997; Kuypers et al., 2003) and denitrification (Kuenen and Robertson, 1988). It is possible to explore past changes in anammox activity in the sedimentary record using the unique ladderane fatty acids (Sinninghe Damste et al., 2002) but these are relatively poorly preserved in sediments (Jaeschke et al., 2007). Alternatively, the ratio of bacteriohopanetetrol (BHT)-34S (which is ubiquitously synthesized by aerobic bacteria) and the later eluting stereoisomer BHT-x (which is predominately synthesized by marine anammox bacteria, i.e., Ca. Scalindua spp.) (Rush et al., 2014; Schwartz-Narbonne et al., 2020; van Kemenade et al., 2023) can be used to trace past anammox activity. Denitrification is performed by a large range of organisms (Knowles, 1982), but at present, there are no associated diagnostic lipid biomarkers (Rush et al., 2017).

In this study, we used lipid biomarkers of microbes widely involved in the N-cycle across various marine and freshwater environments in combination with other geochemical records from a sediment core located in the western Black Sea spanning the last deglaciation and Holocene (~20 ka – present) to better constrain and assess the sensitivity of the marine N-cycle under changing hydrological and oxygenation conditions and explore its potential links to broader global climate dynamics.

2. Regional Setting

The Black Sea is a large meromictic marginal basin connected to the Mediterranean Sea via the Turkish Straits (the Bosporus, the Sea of Marmara, and the Dardanelles Strait) (Fig. 1). The Black Sea has a net outflow into the Aegean Sea via the Turkish Straits, and is primarily supplied by three major rivers, the Danube, Dnieper, and Don. With freshwater flowing out of the basin and dense, highly saline waters flowing in, the water column is highly stratified with respect to salinity (density). An oxygenated colder surface layer (0 – 50 m) overlies warmer, anoxic, sulfidic, hypersaline deep waters (100 – 2300 m), separated by a suboxic layer (50 – 100 m) (Murray et al., 1989; 1995). The general circulation of Black Sea surface-waters is a basin-scale cyclonic boundary current encompassing large eastern and western cyclonic gyres, with several smaller, anticyclonic coastal eddies (Fig. 1) (Özsoy and Ünlüata, 1997). The modern Black Sea water column is characterized by the presence of strong redox gradients. In the basin's western gyre, the oxic zone (0 – 75 m depth range) has an oxygen concentration of ~121 µmol/kg and salinity of 19.4 psu at 50 m depth, with no detectable sulfide concentrations (Sollai et al., 2018; Bale et al., 2021). The suboxic zone lies below (75 – 115 m depth range), where salinity increases with depth and

116 traces of sulfide are detected at the bottom of this layer at ~110 m (Sollai et al., 2018; Bale et al., 2021). Beneath

117 this lies the euxinic zone (115 – 2000 m depth range), where salinity and sulfide concentrations increase with

118 depth, reaching 22.3 psu and ~400 μmol/L at a depth of 2,000 m (Sollai et al., 2018; Bale et al., 2021). Ammonium

119 concentrations are low in the oxic and upper suboxic zones (<0.1 μmol/L), increasing below 90 m, with highest

120 concentrations (~100 μmol/L) at 2000 m water depth (Sollai et al., 2018). Nitrite concentrations are highest in

121 the oxic zone, peaking at 50 m (~0.08 μmol/L), decreasing through the suboxic zone, with the exception of a

122 peak at 85 m, while in the euxinic zone, nitrite is below the limit of detection (Sollai et al., 2018). Nitrate

123 concentrations are highest in the lower oxic and upper suboxic zones, peaking between 70 – 80 m (~2.5 μmol/L),

124 decreasing with depth and reaching the limit of detection below 105 m (Sollai et al., 2018; Bale et al., 2021).

125

126 **3. Methods**

127 During the cruise with the RV Pelagia in April 2017, piston core 64PE418 (235 cm length) was recovered from

128 1970 m below sea level (mbsl) depth in the Black Sea (42°56 N, 30°02 E) (Fig. 1). 44 sediment samples were taken

129 at 5 cm intervals along the depth of the core.

130

131 *3.1. Biomarker extraction and analysis*

132 Lipids were extracted from these samples using a modified Bligh and Dyer extraction method as described

133 previously (Bale et al., 2021). Using a mixture of methanol (MeOH), dichloromethane (DCM), and phosphate

134 buffer (2:1:0.8, v:v), the sediment was twice extracted ultrasonically (10 min). The combined supernatants were

135 phase-separated by adding DCM and phosphate buffer to create a solvent ratio of 1:1:0.9 (v:v). The organic

136 phase was collected, and the aqueous phase re-extracted three times using DCM. All extraction steps were then

137 repeated on the residue but with a mixture of MeOH, DCM and aqueous trichloroacetic acid solution (TCA) pH

138 3 (2:1:0.8, v:v). Finally, the organic extracts were combined and dried under a N_2 gas stream. A deuterated

139 betaine lipid {1,2-dipalmitoyl-sn-glycero-3-O-4'-[N,N,N-trimethyl(d9)]-homoserine; Avanti Lipids} internal

140 standard was added to each sample before filtering the extract through 0.45 μm cellulose syringe filters (4 mm

141 diameter; BGB, USA). Extraction blanks were performed alongside the sediment extractions, using the same

142 glassware, solvents and extraction methodology, but without sediment. Analysis of the extracts was performed

143 using the following UHPLC-HRMS reversed phase method. An Agilent 1290 Infinity I UHPLC was used, equipped

144 with thermostatted auto-injector and column oven, coupled to a Q Exactive Orbitrap MS with Ion Max source

145 using heated electrospray ionization (HESI) probe (Thermo Fisher Scientific, Waltham, MA). Separation was

146 achieved using an Acquity BEH C18 column (Waters, 2.1 × 150 mm, 1.7 μm) maintained at 30°C. The eluent

147 composition was (A) MeOH/H_2O/formic acid/14.8 M NH_3aq [85:15:0.12:0.04 (v:v)] and (B) IPA/MeOH/formic

148 acid/14.8 M NH_3aq [50:50:0.12:0.04 (v:v)]. The elution program was: 95% A (for 3 min) followed by a linear

149 gradient to 40% A (at 12 min) and then to 0% A (at 50 min), which was maintained until 80 min. The flow rate

150 was 0.2 mL min^{-1}. Positive ion HESI settings were: capillary temperature, 300°C; sheath gas (N_2) pressure, 40

151 arbitrary units (AU); auxiliary gas (N_2) pressure, 10 AU; spray voltage, 4.5 kV; probe heater temperature, 50°C;

152 S-lens 70 V. Lipids were analyzed with a mass range of *m/z* 350–2000 (resolving power 70,000 ppm at *m/z* 200),

153 followed by data-dependent tandem MS/MS (resolving power 17,500 ppm), in which the 10 most abundant

masses in the mass spectrum were fragmented successively. Optimal fragmentation was achieved with a stepped normalized collision energy of 15, 22.5 and 30 (isolation width, 1.0 m/z) for IPL analysis (Bale et al., 2021) and 22.5 and 40 (isolation width 1.0 m/z) for BHP analysis (Hopmans et al., 2021). The Q Exactive was calibrated within a mass accuracy range of 1 ppm using the Thermo Scientific Pierce LTQ Velos ESI Positive Ion Calibration Solution. During analysis, dynamic exclusion was used to temporarily exclude masses (for 6 s) to allow selection of less abundant ions for MS/MS.

Biomarkers were identified based on their retention time, exact mass, and fragmentation spectra. Integrations were performed on (summed) mass chromatograms of relevant molecular ions ([M+H]$^+$, [M+NH4]$^+$, and [M+Na]$^+$) and in the case of crenarchaeol also the second isotope peak for each of the three adducts. Due to coelution of BHT-34S, BHT-x isomer and an unknown nitrogen containing compound with the same mass, identification and integration of BHT-34S and BHT-x was conducted using the m/z 529.462 dehydrated insource product ([M+H]$^+$-H_2O). Isoprenoidal glycerol dialkyl glycerol tetraether (isoGDGT) crenarchaeol, monohexose crenarchaeol, and a crenarchaeol isomer were all integrated and combined as 'crenarchaeol'. The lipid biomarker records are all presented as peak area per gram of total organic carbon (TOC).

3.2. Total organic carbon and total nitrogen and $\delta^{15}N_{bulk}$ measurements

Freeze-dried sediments were analysed for TOC, total nitrogen (TN) and bulk $\delta^{15}N$ ($\delta^{15}N_{bulk}$) using a ThermoScientific Flash EA Delta V Plus IRMS. Flow was 100 ml/min and the temperature for oxidation, reduction and the oven were 900°C, 680°C, and 40°C, respectively. Nitrogen isotopic measurements were calibrated to atmospheric air (AIR) and values are expressed in permil (‰) units. Inorganic carbon was removed from the sediment prior to TOC analysis using HCl (2 mol), cleaned with bi-distilled water, then freeze-dried.

3.3. Age model

Accelerator Mass Spectrometry (AMS) ^{14}C ages of bulk organic matter were measured from core 64PE418 (n = 7) to create a chronology on the 64PE418 depth scale. Samples were weighed and freeze-dried at NIOZ. The AMS ^{14}C measurements ($^{14}C/^{12}C$) were determined using a Compact Carbon AMS System at the Poznań Radiocarbon Laboratory, Poland. The sediment samples were pre-treated with 0.25M HCl (room temperature overnight, then 80°C, 1+ hour), and rinsed with deionised water until pH = 7. Samples were then combusted in closed (sealed under vacuum) quartz tubes, together with CuO and Ag wool (900°C, 10 hours). The CO_2 released was then dried in a vacuum line and reduced with H_2 using 2 mg of iron (Fe) powder as a catalyst. The obtained carbon and Fe mixture was then pressed into an aluminium holder (Czernik & Goslar, 2001). The measurement was performed by comparing intensities of ionic beams of ^{14}C, ^{13}C and ^{12}C measured for each sample and for standard samples (with "Oxalic Acid II" used as modern standard; "coal" used as background standard of ^{14}C-free carbon). In each AMS run, 30-33 samples of unknown age were measured, alternated with measurements of 3-4 samples of modern standard and 1-2 samples of background standard. The measured $^{14}C/^{12}C$ ratios are corrected for isotopic fractionation and reported as conventional radiocarbon age according to Stuiver & Polach (1977).

192

193   Seven bulk organic matter ^{14}C dates were used in the production of the age-model for core 64PE418 (Table S1

194   and Fig. S1). Six of these were from this core, with an additional bulk organic carbon ^{14}C date from the widely

195   acknowledged Unit I/II boundary of core KNR 134-08 BC17, which was used to further refine the age model for

196   the upper part of the core (Jones & Gagnon, 1994). Core KNR 134-08 BC17 was sourced from the same location

197   and water depth as 64PE418 and this boundary was identified in our core using the same significant colour and

198   elemental changes described in previous studies (Fig. 2 and 3) (i.e., Arthur & Dean, 1998; Bahr et al., 2005).

199   While seven ^{14}C measurements were conducted on core 64PE418, one was excluded from the age model due to

200   an age reversal (142.5 cm), likely due to the presence of reworked material, which would have made the age

201   model out of line with other studies (Fig. S2). Variable reservoir-ages were added to our calibration (Table S1),

202   using those calculated by Kwiecien et al., (2008) for intermediate water depths in the Black Sea over the last

203   deglaciation and Holocene which were deemed the most suitable for our site location. The ^{14}C dates were

204   calibrated using the Marine20 calibration curve (Heaton et al., 2020) for the upper three samples (24.5, 39, 76.5

205   cm) which reflect the period after the infiltration of marine water; this is based on the colour and elemental

206   changes in the core which indicate that these samples fall within Units I and II (Arthur & Dean, 1998; Bahr et al.,

207   2005). The lower four samples (118.5, 158.5, 183.5 and 217.5 cm) were calibrated using the IntCal20 calibration

208   curve (Reimer et al., 2020), as they reflect the period prior to the marine infiltration when then Black Sea was a

209   lacustrine environment, as indicated by colour and elemental signatures in the core (Arthur & Dean, 1998; Bahr

210   et al., 2005). Using the R-code CLAM (Blaauw, 2010), the age–depth model was created based on the seven [14]C

211   dates. Our age model shows that the 64PE418 biomarker records span the last 19.5 ka, with an average

212   resolution of ~450 years. The following transitions are identified in our core by colour (Fig. 2) and elemental

213   changes (Fig. 3) and dated by our age model as follows: the onset of the IMI (138 cm) is at 9.6 ka ± 237 yrs, the

214   boundary of Unit II/III (96 cm) is dated at 7.2 ka ± 202 yrs, and the Unit I/II boundary (39 cm) is dated at 2.6 ka ±

215   402 yrs. Despite the complexity of dating Black Sea cores, due to lack of suitable material for dating and dispute

216   over reservoir age corrections (Kwecien et al., 2008; Soulet et al., 2011; Yanchilina et al. 2017), the dates of these

217   boundaries align well with previously published calibrated ages for these transitions (i.e., Jones & Gagnon, 1994;

218   Ankindinova et al., 2019; Huang et al., 2021), as shown in Fig. S2.

219

220   **4. Results**

221

222   ***4.1. TOC, TN and colour changes***

223   Sedimentary bulk TOC (%), bulk TN (%), and $\delta^{15}N_{bulk}$ (‰) range between 0.3 – 22.8% for TOC and 0.05 – 1.9% for

224   TN, and 5.2 – 0.0‰ for $\delta^{15}N_{bulk}$ (Fig. 4). There are significant colour changes in the core, as shown in Fig. 2 which

225   correspond to changes in TOC, TN and the elemental composition (Fig. 3). In the lower part of the core (19.5 –

226   9.6 ka), values are relatively low for TOC and TN, at ~0.84% and ~0.10%, respectively. At 9.6 ka, there is an

227   appreciable change in the elemental composition of the core, with increases in Ti/Ca, K and V and a decrease in

228   Mn/Al, which corresponds with a transition to darker sediments and an increase in TOC and TN to ~2.41% and

229   ~0.26%, respectively. At 7.2 ka there is another major change in the colour and bulk elemental composition of

230   the core, with an increase in redox-sensitive elements U, V, and Mo and a decrease in Ti/Ca and K (Fig. 3), which

231   corresponds with darker sediments and increasing TOC values. TOC peaks between 6.6 – 4.6 ka (~21% for TOC

232   and ~1.7% for TN), declining towards the top of the core. $\delta^{15}N_{bulk}$ shows a general decline in values from the

233   upper to the lower part of the core. This decline is small between 19.5 – 7.7 ka (4.9 – 3.3‰), before a more

234   significant decrease to 1.2‰ at 6.6 ka (3.3 – 1.2‰). Values increase to 3.7‰ at 6.1 ka before declining to 0.0‰

235   at 3.9 ka, increasing slightly towards the top of the core to values of 1.3‰.

236

237   *4.2. Biomarkers*

238   We examined a number of lipid biomarkers related to the N-cycle in Black Sea core 64PE418 (Fig. 4). HGs were

239   identified in all samples (with the exception of 215 cm (16.4 ka)). These include HGs with a hexose (C_6) headgroup

240   i.e., hexose C_{26} diol, hexose C_{28} diol, hexose C_{28} triol and hexose C_{30} triol, which are specific to free-living

241   cyanobacteria, found in predominately freshwater and brackish environments (Bauersachs et al, 2009; Wörmer

242   et al., 2012). In addition, those with a pentose (C_5) headgroup i.e., pentose C_{30} diol, pentose C_{30} triol, pentose

243   C_{32} triol were detected which are specific to cyanobacteria symbiotic with marine diatoms (Schouten et al., 2013;

244   Bale et al., 2015). Hexose HGs are present throughout the core, increasing substantially in abundance between

245   9.6 – 6.6 ka, reaching maximum values at 9.6 ka. Pentose HGs are detected from 4.3 ka onwards, increasing in

246   abundance at the top of the record coinciding with low abundance of hexose HGs. Crenarchaeol, a marker for

247   Thaumarchaeota, was identified throughout our record, showing high values in the early part of the record (~

248   1.1E+14 peak area per g TOC) until 6.9 ka, abruptly shifting to lower values ~ 3.9E+13 peak area per g TOC

249   thereafter. The BHT-x ratio, a biomarker for anammox bacteria, is low in the early part of our record (<0.3), due

250   to low abundance of BHT-x. The BHT-x ratio increases after 6.9 ka to values around 0.3, due to higher abundance

251   of BHT-x and lower abundance of BHT with a 34S stereoconfiguration.

252

253   Finally, to reconstruct levels of oxygen in the subsurface waters of the Black Sea, isorenieratene was identified

254   (as described in Bale et al., 2021). Isorenieratene is a marker of the brown-coloured strains of the photosynthetic

255   green sulfur bacteria, Chlorobiaceae, which are anoxygenic photoautotrophs that require light and hydrogen

256   sulphide (H_2S); their presence indicates photic zone euxinia, whereby anoxic, sulfidic waters reached the photic

257   zone (Sinninghe Damste et al., 1993; Koopmans et al., 1996). Isorenieratene was identified in many of our

258   samples after 9.5 ka, peaking between 5.6 – 4.3 ka (reaching 3.39E+12 per g TOC at 5.6 ka), but was not detected

259   between 3.9 – 2.7 ka.

260

261   **5. Discussion**

262   Based on clear changes in TOC (Fig. 4), colour and elemental signatures (Fig. 2 and 3), we divided core 64PE418

263   into three widely acknowledged units, in line with previous studies (Jones & Gagnon, 1994; Arthur & Dean, 1998;

264   Bahr et al., 2005). Unit III spans ~20 – 7.2 ka, covering the period where the Black Sea was a lacustrine

265   environment, disconnected from the global ocean, and also the transition interval, where the basin moved

266   towards a marine environment after the IMI over the Bosporus sill at ~9.6 ka (Aksu et al., 2002; Major et al.,

267   2006; Bahr et al., 2008; Ankindinova et al., 2019). Unit II (~7.2 – 2.6 ka) and Unit I (~2.6 ka - present) span the

period where the Black Sea had become an anoxic brackish-to-marine environment. Diagenesis and preservation biases can affect lipid biomarker records, but since the records do not all mirror the oxygenation of the water column, and organic carbon contents remained relatively high, it is unlikely that diagenesis and preservation significantly influenced these records.

5.1. Oxic lacustrine phase (19.5 – 9.6 ka)

Throughout the last deglaciation and early Holocene (19.5 – 9.6 ka), TOC and TN levels are low, likely due to poor preservation of organic material, caused by the well-ventilated, oxygenated, freshwater environment that existed in the basin at this time (Schrader, 1979). Isorenieratene is not detected during this period, while elements that accumulate in sediment under anoxic conditions (i.e., Algeo and Li, 2020) also remained low (i.e., U, V, Mo; Fig. 2), which all points to a well-oxygenated environment. Freshwater/brackish conditions prevailed throughout this time, as shown by previous studies (Fig. S3; Filipova-Marinova et al., 2013; Ion et al., 2022; Huang et al., 2022). Throughout this period, the abundance of Thaumarchaeota, indicated by crenarchaeol abundance, and anammox, indicated by the BHT-x ratio, remained relatively steady (Fig. 4). This stability is remarkable since the region experienced significant climatic changes which led to large variations in the surface water temperatures of the Black Sea, varying from $\sim$10$°$C during the Bølling Allerød, $\sim$7$°$C during the Younger Dryas and $\sim$14$°$C by the Early Holocene (Ménot & Bard, 2012), as well as changes in the input of freshwater into the basin due regional precipitation variability and the melting of Eurasian icesheets and alpine glaciers (Bahr et al., 2005; 2006; 2008; Badertscher et al., 2011; Shumilovskikh et al., 2012; Filipova-Marinova et al., 2013; Ion et al., 2022). The subsurface stability is likely due to the stratification of the basin, where significant climatic shifts primarily impacted the surface waters, and the limited vertical mixing minimised the influence on subsurface waters, creating a stable environment for the subsurface nitrogen cycle. In contrast, changes in HG abundance and distribution suggest that surface-dwelling nitrogen-fixing cyanobacteria were sensitive to surface-water hydrological changes in the Black Sea over this period (Fig. 5). The dominant HG structure varies between hexose C_{26} diol, hexose C_{28} diol and hexose C_{30} triol and after 11 ka, hexose C_{28} triol becomes present, which has been shown to be the major HG in members of the Rivulariaceae family (i.e., Calothix sp.) (Bauersachs et al., 2009). The warmer wetter conditions of the Early Holocene may have provided a trigger for this change in HG abundance and composition. Indeed, an increase in the abundance of the genus *Rivularia* was also noted in coastal regions of SW India during this period, coinciding with an increasingly warm and wet climate (Limaye et al., 2017). Another cause for this shift may have been related to changes in nutrient availability, with members of the Rivulariaceae family typically occurring in environments with highly variable phosphorus availability (Whitton & Mateo, 2012).

5.2. Transition phase (9.6 – 7.2 ka)

In line with existing research (Arthur & Dean, 1998; Bahr et al., 2006; 2008), the IMI occurred at $\sim$9.6 ka, leading to a significant change in colour (Fig. 2) and elemental composition of the sedimentary record (Fig. 3), as well as a substantial increase in abundance of HGs (Fig. 4). This increase does not coincide with higher TOC content, suggesting that enhanced preservation of HGs was not the cause. It is possible that these lipid biomarkers were

transported fluvially to this site from lakes within the catchment basin of the Black Sea due to the warm/wet conditions at this time (Göktürk et al., 2011; Shumilovskikh et al., 2012; Filipova-Marinova et al., 2013). This, however, appears unlikely as our site is located a substantial distance from the mouths of major rivers (>230 km), and the BIT index remains low during this period (~0.08; pers. comms. B.Yang), indicating only a minor contribution of terrestrial organic matter at our site (Hopmans et al., 2004). Furthermore, as the proceeding period (7 – 5.6 ka) was also warm and wet (Göktürk et al., 2011; Shumilovskikh et al., 2012; Filipova-Marinova et al., 2013), we would expect the continuation of this peak if the HGs were being sourced from surrounding lacustrine environments. Instead, these high values decline abruptly after 6.6 ka.

It is therefore likely that the peak abundance in nitrogen-fixing cyanobacteria is related to warmer Black Sea surface temperatures during the early to mid-Holocene (Bahr et al., 2008) in combination with surface water stratification (Bahr et al., 2006). This stratification will have slowed the upward supply of fixed nitrogen, reducing nutrient availability in the surface waters, thereby promoting nitrogen-fixation by cyanobacteria (Hutchins & Fu, 2017). This stratification may have been driven in part by enhanced freshwater influx due to wetter conditions but may also have been triggered by the IMI through the Bosporus Strait at ~9.6 ka (Major et al., 2006; Bahr et al., 2008; Ankindinova et al., 2019). This IMI likely led to the gradual salinisation of the water column over this transition interval and intermittent build-up of anoxia in the water column. This, in turn, led to periods of higher preservation of organic matter compared to the preceding period, as indicated by the slight increase in TOC after 9.6 ka. The presence of isorenieratene after 9.4 ka indicates that anoxia reached the photic zone at intermittent periods during this transition interval, thereby providing sufficient conditions for the presence of the anoxygenic photoautotrophs, Chlorobiaceae. While the peak in nitrogen-fixing cyanobacteria occurs ~2 ka before anoxia intermittently entered the photic zone, the initial influx of dense saline water may have led to some reduction in vertical circulation, which reduced the amount of fixed nitrogen upwelled to the upper water column, leading to the presence of nitrogen-fixing cyanobacteria at 9.6 ka. This also coincides with a change in the distribution of HGs in our record between 9.7 – 6.9 ka where hexose C_{28} diol and hexose C_{30} triol increase in abundance and hexose C_{28} triol declines in relative abundance and is no longer present after 9.1 ka, coinciding with the presence of isorenieratene. These changes may reflect a shift in species composition, linked to the gradual salinisation and periodic anoxification of the water column after the IMI. The IMI at ~9.6 ka appears, however, to have had little impact on the abundances of anammox and Thaumarchaeota. This is possibly because basin-wide water column stratification and the permanent build-up of anoxia did not occur until later in the record, meaning that neither process instantaneously reacted to the IMI at ~9.6 ka.

5.3. Shift to anoxic brackish-to-marine mode of operation: a critical N-cycle threshold (~7.2 ka to present)

After 7.2 ka there was a substantial increase in TOC and TN and an abrupt shift in parts of the subsurface N-cycle. The latter is shown by an increase in the BHT-x ratio, indicating an intensification of anammox, which is coeval with a decrease in crenarchaeol, indicating that there was a decline in Thaumarchaeota-driven nitrification. Studies have shown that by ~7.2 ka anoxia had built up in the water column, as indicated by changes in redox elements (Fig. S2 and Eckert et al., 2013; Wegwerth et al., 2018) and water column salinity had

344   significantly increased (Fig. S3; Hiscott et al., 2007; Marret et al., 2009; Soulet et al., 2011; Filipova-Marinova et

345   al., 2013), following the IMI from the Sea of Marmara at ~9.6 ka (Major et al., 2002; 2006; Bahr et al., 2005;

346   2008; Ankindinova et al., 2019). This is supported by the presence of isorenieratene in our record during this

347   time, which indicates that anoxia penetrated the photic zone. This water column anoxia likely led to the

348   enhanced preservation of TOC and TN and triggered a shift in the subsurface N-cycle, which crossed a threshold

349   from an oxygenated lacustrine mode of operation to an anoxic brackish-to-marine mode of operation. The

350   anoxic water column enabled anammox bacteria to expand their habitat from the anoxic sediments, where they

351   likely were confined when the basin was an oxygenated freshwater environment, up into the suboxic/anoxic

352   water column. This may therefore have commenced part of the modern-day N-cycle in the Black Sea where

353   anammox activity occurs in the lower suboxic zone (~100 mbsl) where O_2 is (near) depleted and H_2S is absent

354   (Jensen et al., 2008), with anammox bacteria consuming ammonium diffusing from the deep sea and utilising

355   the nitrite produced by both Thaumarchaeota and ammonia-oxidising bacteria (AOB) (Kuypers et al., 2003; Lam

356   et al., 2007). Consequently, it may be that the abundance of anammox bacteria increased as a result of the

357   coupling to nitrite production by other microbes in the suboxic zone, whilst benefitting from ammonium

358   diffusing upwards from the deep sea. The increased anammox after 7.1 ka likely indicates that more bioavailable

359   nitrogen was lost from the system after the switch to the anoxic brackish-to-marine mode of operation. At the

360   same time, Thaumarchaeota abundance declined, which may be in part due to the build-up of anoxia in the

361   water column which reduced the niche of these aerobic microbes and the nitrification performed by them. Once

362   these processes crossed a threshold from an oxygenated lacustrine mode of operation to an anoxic brackish-to-

363   marine mode of operation, they appear to have remained steady for the remainder of the Holocene despite

364   changes in the salinity of the basin (van der Meer et al., 2008; Mertens et al., 2012; Coolen et al., 2013) and

365   significant changes in regional temperature and precipitation (Göktürk et al., 2011; Shumilovskikh et al., 2012;

366   Filipova-Marinova et al., 2013). This shows that deoxygenation was the main driver of the observed change in

367   annamox as well as archaeal nitrification and that they were not affected by hydrological changes mainly

368   occurring at the surface. While our record shows centennial-scale changes in the N-cycle, we acknowledge that

369   there may have also been rapid or short-term variations in N-cycle dynamics over this period that may not have

370   been captured by the resolution of this record.

371

372   At 6.1 ka, the abundance of the HGs substantially declined, coinciding with an increase in $\delta^{15}N_{bulk}$, indicating a

373   reduction in nitrogen fixation. This corresponds with the high-resolution record of Fulton et al., (2012) which

374   also shows a decline in values at this time. As this decline in HG abundance and increase in $\delta^{15}N_{bulk}$ does not

375   coincide with a reduction in TOC, it is unlikely that reduced preservation of HGs played a role here. As nitrogen-

376   fixing cyanobacteria inhabit the upper surface layer, it is likely that this change is linked to the salinisation of the

377   surface waters, with many studies demonstrating the disappearance of many freshwater mollusc, ostracod and

378   dinoflagellate cyst species at this time, which were replaced by an increased abundance of euryhaline

379   Mediterranean species (Hiscott et al., 2007; Marret et al., 2009; Filipova-Marinova et al., 2013; Ivanova et al.,

380   2015). At 6.1 ka, hexose C_{26} diol and hexose C_{28} diol are the only HGs present in the record, which may reflect

381   the dominance of genera in the Nostocaceae family (i.e., Anabaena sp., Aphanizomenon sp., Nodularia sp.,

382   Nostoc sp.), as these members demonstrate a dominance of the hexose C_{26} diol and also contain varying

383   amounts of hexose C_{28} diol (Gambacorta et al., 1999; Bauersachs et al., 2009). This distribution is similar to that

384   of the Baltic Sea after ~7.2 ka when a series of weak intrusions of saline water led to the basin becoming fully

385   brackish (Sollai et al., 2017). It is therefore possible that the peak in HGs in our Black Sea record between 9.6 –

386   6.9 ka represents a transition from the dominance of freshwater tolerant nitrogen-fixing cyanobacteria to more

387   brackish species, with brackish species dominating the surface-waters after 6.6 ka. After 6.1 ka, $\delta^{15}N_{bulk}$ gradually

388   decreases, indicating a rise in nitrogen fixation, with this pattern also shown in previous records (Blumenberg et

389   al., 2009; Fulton et al., 2012). While previous studies have shown riverine nitrogen to be a major source of fixed

390   nitrogen in the modern Black Sea (McCarthy et al., 2007), due to the remoteness of our core site from the coast,

391   our records are unlikely to have been significantly influenced by riverine input. It should be noted that a previous

392   study (Fulton et al., 2012) suggested, based on compound specific measurements of pyropheophytin, that

393   sedimentary $\delta^{15}N$ in the Black Sea is primarily derived from eukaryotic algae rather than cyanobacteria which

394   exhibits a different fractionation of nitrogen isotopes . This means the use of $\delta15N_{bulk}$ as a nitrogen fixation signal

395   must be used with caution. HGs, however, are only derived from N-fixing cyanobacteria and are therefore an

396   unambiguous biomarker of nitrogen fixation. Interestingly, at 4.3 ka pentose HGs are detected, coinciding with

397   lowest $\delta^{15}N_{bulk}$, indicating the presence of marine nitrogen-fixing cyanobacteria found in symbiosis with marine

398   diatoms. This indicates that the surface water salinity had reached a threshold which enabled these marine

399   microbes to survive, with research indicating salinity reached ~17‰ during the deposition of Unit I (Ion et al.,

400   2022) and freshwater/brackish species had disappeared by this time (Fig. S3; Filipova-Marinova et al., 2013).

401   Indeed, reported increases in the number of euryhaline species at this time also points to the increasing salinity

402   of the surface waters (Marret et al., 2009; Bradley et al., 2012), which may be linked to warmer/drier conditions

403   which reduced freshwater influx and/or enhanced evaporation (Göktürk et al., 2011). Between 3.9 – 2.7 ka,

404   isorenieratene is not detected in the samples, reflecting the findings of previous studies (Sinninghe Damsté et

405   al., 1993). It has been suggested that this resulted from the erosion of the chemocline (Sinninghe Damsté et al.,

406   1993), while other research shows a short reoccurrence of freshwater/brackish species (Fig. S3; Filipova-

407   Marinova et al., 2013), which may indicate that enhanced freshwater input was responsible for lowering the

408   chemocline below the photic zone. The disappearance of hexose HGs after 0.6 ka indicates that surface water

409   salinities may more recently have become too high for the proliferation of brackish nitrogen-fixing

410   cyanobacteria.

411

412   **6. Conclusions**

413   This study shows a relatively stable subsurface N-cycle in the Black Sea over the last deglaciation and Holocene

414   with the exception of a critical threshold observed at 7.2 ka when the basin shifted from an oxygenated

415   lacustrine environment to an anoxic brackish-to-marine basin. At this time, the loss of bioavailable nitrogen

416   through anammox activity was enhanced and Thaumarchaeota-driven nitrification was reduced. Prior to, and

417   after this transition, the subsurface N-cycle was remarkably stable despite various climatic and hydrological

418   changes that impacted the basin during the deglaciation and Holocene periods. Both the amount of nitrogen

419   fixation by cyanobacteria and the composition of these microbes in the surface waters, however, appear to be

420 much more dynamic and sensitive to hydrological changes over this period, responding in particular to salinity
421 and temperature changes and stratification of the water column. Consequently, these records provide
422 important insight into how future deoxygenation in marine environments may affect the microorganisms
423 involved in the N-cycle, possibly leading to enhanced loss of bioavailable nitrogen by anammox, and reduced
424 nitrification by Thaumarchaeota. Furthermore, in areas where enhanced water column stratification limits the
425 supply of fixed nitrogen in the surface waters, localised enhanced cyanobacterial nitrogen fixation in the surface
426 waters may occur. These changes may have associated feedbacks on nutrient cycling and carbon fixation, with
427 implications for the future global carbon budget.
428

429 **Data Availability**
430 All data generated for this study are archived and publicly available via the Mendeley Data repository online at
431 https://10.17632/4c9fg7jf5d.1 (Cutmore et al., 2024).
432

433 **Acknowledgements**
434 We thank the Chief Scientist Prof. Laura Villanueva as well as the captain and crew of the *R/V* Pelagia for the
435 collection of core 64PE418. We would like to thank Jaap Sinninghe Damsté for useful discussions. For laboratory
436 support we thank Anchelique Mets, Denise Dorhout and Monique Verweij. Research cruise 64PE418 was funded
437 by the SIAM Gravitation Grant (024.002.002) from the Dutch Ministry of Education, Culture and Science (OCW).
438 This study was funded by the Netherlands Earth System Science Centre (024.002.001) from the Dutch Ministry
439 of Education, Culture and Science (OCW).

440

441 **Author Contributions**
442 Anna Cutmore: Conceptualization, Formal analysis, Investigation, Data Curation, Visualization, Writing - Original
443 Draft, Writing - Review & Editing; Nicole Bale: Conceptualization, Methodology, Investigation, Supervision,
444 Writing - Review & Editing; Rick Hennekam: Resources, Formal analysis, Investigation, Writing - Review & Editing;
445 Darci Rush: Formal analysis, Writing - Review & Editing; Bingjie Yang: Formal analysis, Investigation, Writing -
446 Review & Editing; Gert-Jan Reichart: Resources, Supervision, Writing - Review & Editing; Ellen C. Hopmans:
447 Supervision; Stefan Schouten: Conceptualization, Supervision, Funding acquisition, Writing - Review & Editing

448

449 **Competing interests:** The authors declare that they have no conflict of interest.
450

451 **References:**
452

453 Aksu, A., Hiscott, R.N., Kaminski, M.A., Mudie, P.J., Gillespie, H., Abrajano, T and Yasar, D. 2002. Last glacial–
454 Holocene paleoceanography of the Black Sea and Marmara Sea: stable isotopic, foraminiferal and coccolith
455 evidence. *Marine Geology*, **190**, 119-149. doi.org/10.1016/S0025-3227(02)00345-6

456

457 Algeo, T.J and Li, C. 2020. Redox classification and calibration of redox thresholds in sedimentary systems.

458 *Geochimica et Cosmochimica Acta*, **287**, 8-26. doi.org/10.1016/j.gca.2020.01.055

459

460 Ankindinova, O., Hiscott, R.N., Aksu, A.E and Grimes, V. 2019. High-resolution Sr-isotopic evolution of Black Sea

461 water during the Holocene: Implications for reconnection with the global ocean. *Marine Geology*, **407**, 213-228.

462 doi.org/10.1016/j.margeo.2018.11.004

463

464 Arthur & Dean, 1998. Organic-matter production and preservation and evolution of anoxia in the Holocene Black

465 Sea. *Palaeoceanography & Palaeoclimatology,* **13**, 395-411. doi.org/10.1029/98PA01161

466

467 Badertscher, S., Fleitmann, D., Cheng, H., Edwards, R.L., Göktürk, O.M., Zumbühl, A., Leuenberger, M and Tüysüz,

468 O. 2011. Pleistocene water intrusions from the Mediterranean and Caspian seas into the Black Sea. *Nature*

469 *Geoscience*, **4**, 236–239. doi.org/10.1038/ngeo1106

470

471 Bale, N., Hopmans, E.C., Zell, C., Sobrinho, R.L., Kim, J.-H., Sinninghe Damsté, J.S., Villareal, T.A and Schouten, S.

472 2015. Long chain glycolipids with pentose head groups as biomarkers for marine endosymbiotic heterocystous

473 cyanobacteria. *Organic Geochemistry*, **81**, 1-7. doi.org/10.1016/j.orggeochem.2015.01.004

474

475 Bale, N.J., Hennekam, R., Hopmans, E.C., Dorhout, D., Reichart, G.-J., van der Meer, M.T.J., Villareal, T.A.,

476 Sinninghe Damsté, J.S and Schouten, S. 2019. Biomarker evidence for nitrogen-fixing cyanobacterial blooms in a

477 brackish surface layer in the Nile River plume during sapropel deposition. *Geology*, **47**, 1088–1092.

478 doi.org/10.1130/G46682.1

479

480 Bale, N., Ding, S., Hopmans, E.C., Arts, M.G.I., Villanueva, L., Boschman, C., Haas, A.F., Schouten, S and Sinninghe

481 Damsté, J.S. 2021. Lipidomics of Environmental Microbial Communities. I: Visualization of Component

482 Distributions Using Untargeted Analysis of High-Resolution Mass Spectrometry Data. Frontiers in Microbiology,

483 **12**, 1-15. doi.org/10.3389/fmicb.2021.659302

484

485 Bahr, A., Lamy, F., Arz, H., Kuhlmann, H and Wefer, G. 2005. Late glacial to Holocene climate and sedimentation

486 history in the NW Black Sea. *Marine Geology*, **214**, 309-322. doi.org/10.1016/j.margeo.2004.11.013

487

488 Bahr, A., Arz, H., Lamy, F and Wefer, G. 2006. Late glacial to Holocene paleoenvironmental evolution of the Black

489 Sea, reconstructed with stable oxygen isotope records obtained on ostracod shells. *Earth and Planetary Science*

490 *Letters Volume*, **241**, 863-875. doi.org/10.1016/j.epsl.2005.10.036

491

492 Bahr, A., Lamy, F., Arz, H., Major, C., Kwiecien, O and Wefer, G. 2008. Abrupt changes of temperature and water

493 chemistry in the late Pleistocene and early Holocene Black Sea. *Geochemistry, Geophysics, Geosystems*, **9**, 1-16.

494 http://doi.org/10.1029/2007GC001683

495

496 Bauersachs, T., Compaoré, J., Hopmans, E.C., Stal, L.J., Schouten, S and Sinninghe Damsté, J. 2009. Distribution

497 of heterocyst glycolipids in cyanobacteria. *Phytochemistry*, **70**, 2034-2039.

498 doi.org/10.1016/j.phytochem.2009.08.014

499

500 Bauersachs, T., Speelman, E.N., Hopmans, E.C., Reichart, G.-J., Schouten, S and Sinninghe Damsté, J. 2010.

501 Fossilized glycolipids reveal past oceanic N2 fixation by heterocystous cyanobacteria. *Earth & Planetary Science*

502 *Letters*, **107**, 19190-19194. doi.org/10.1073/pnas.1007526107

503

504 Blaaw, M. 2010. Methods and code for 'classical' age-modelling of radiocarbon sequences. *Quaternary*

505 *Geochronology*, **5**, 512-518. doi.org/10.1016/j.quageo.2010.01.002

506

507 Blumenberg, M., Seifert, R., Kasten, S., Bahlmann, E and Michaelis, W. 2009. Euphotic zone bacterioplankton

508 sources major sedimentary bacteriohopanepolyols in the Holocene Black Sea. *Geochimica et Cosmochimica*

509 *Acta*, **73**, 750-766. doi.org/10.1016/j.gca.2008.11.005

510

511 Bopp, L., Resplandy, L., Orr, J.C., Doney, S.C., Dunne, J.P., Gehlen, M., Halloran, P., Heinze, C., Ilyina, T., Séférian,

512 R., Tjiputra, J and Vichi, M. 2013. Multiple stressors of ocean ecosystems in the 21st century: projections with

513 CMIP5 models. *Biogeosciences*, **10**, 6225–6245. doi.org/10.5194/bg-10-6225-2013

514

515 Bradley, L.R., Marret, F., Mudie, P. J., Aksu, A.E and Hiscott, R. N. 2012. Constraining Holocene sea-surface

516 conditions in the south-western Black Sea using dinoflagellate cysts. *Journal of Quaternary Science*, **27**, 835-843.

517 doi.org/10.1002/jqs.2580

518

519 Coolen, M.J.L., Orsib, W.D., Balkema, C., Quince, C., Harris, K., Sylva, S.P., Filipova-Marinova, M and Giosan, L.

520 2013. Evolution of the plankton paleome in the BlackSea from the Deglacial to Anthropocene. *PNAS*, **110**, 8609–

521 8614. doi.org/10.1073/pnas.1219283110

522

523 Czernik, J and Goslar, T. 2001. Preparation of Graphite Targets in the Gliwice Radiocarbon Laboratory for AMS

524 14C Dating. *Radiocarbon*, **43**, 283–291. doi.org/10.1017/S0033822200038121

525

526 Dalsgaard, T., Thamdrup, B., Farías, L and Revsbech, N.P. 2012. Anammox and denitrification in the oxygen

527 minimum zone of the eastern South Pacific. *Limnology & Oceanography*, **57**, 1331-1346.

528 doi.org/10.4319/lo.2012.57.5.1331

529

530 Eckert, S., Brumsack, H.-J., Severmann, S., Schnetger, B., März, C and Fröllje, H. 2013. Establishment of euxinic

531 conditions in the Holocene Black. *Geology*, **41**, 431–434. doi.org/10.1130/G33826.1

532

533 Elling, F.J., Hemingway, J.D., Kharbush, J.J., Becker, K.W., Polik, C.A and Pearson, A. 2021. Linking diatom-
534 diazotroph symbioses to nitrogen cycle perturbations and deep-water anoxia: Insights from Mediterranean
535 sapropel events. *Earth and Planetary Science Letters*, **571**, 1-11. doi.org/10.1016/j.epsl.2021.117110

537 Falkowski, P.G., Barber, R.T and Smetacek, V. 1998.Biogeochemical controls and feedbacks on ocean primary
538 production. *Science*, **281**, 200-206. doi.org/10.1126/science.281.5374.20

540 Filipova-Marinova, M., Pavlov, D., Coolen, M and Giosan, L. 2013. First high-resolution marinopalynological
541 stratigraphy of Late Quaternary sediments from the central part of the Bulgarian Black Sea area. *Quaternary*
542 *International*, **293**, 170-183. doi.org/10.1016/j.quaint.2012.05.002

544 Francis, C.A., Roberts, K.J., Beman, J.M., Santoro, A.E., Oakley, B.B. 2005. Ubiquity and diversity of ammonia-
545 oxidizing archaea in water columns and sediments of the ocean. *Proceedings of the National Academy of*
546 *Sciences of the USA*, **102**, 14683-14688. doi.org/10.1073/pnas.050662510

548 Fulton, J.M., Arthur, M.A and Freeman, K.H. 2012. Black Sea nitrogen cycling and the preservation of
549 phytoplankton δ15N signals during the Holocene. *Global Biogeochemical Cycles*, **26**, 1-15.
550 doi.org/10.1029/2011GB004196

552 Gambacorta, A., Trincone, A., Soriente, A and Sodano, G. 1999. Chemistry of glycolipids from the heterocysts of
553 nitrogen-fixing cyanobacteria. *Phytochemistry*, **2**, 145–150.

555 Göktürk, O.M., Fleitmann, D., Badertscher, S., Cheng, H., Edwards, R.L., Leuenberger, M., Fankhauser, A., Tüysüz,
556 O and Kramers, J. 2011. Climate on the southern Black Sea coast during the Holocene: implications from the
557 Sofular Cave record. *Quaternary Science Reviews*, **30**, 2433-2445. doi.org/10.1016/j.quascirev.2011.05.007

559 Heaton, T.J., Köhler, P., Butzin, M., Bard, E., Reimer, R.W., Austin, W.E.N., Bronk Ramsey, C., Grootes, P.M.,
560 Hughen, K.A., Kromer, B., Reimer, P.J., Adkins, J., Burke, A., Cook, M.S., Olsen, J and Skinner, L.C. 2020.
561 Marine20—The Marine Radiocarbon Age Calibration Curve (0–55,000 cal BP). *Radiocarbon*, **62**, 779–820.
562 doi.org/10.1017/RDC.2020.68

564 Hennekam, R., van der Bolt, B., van Nes, E.H., de Lange, G.-J., Scheffer, M and Reichart, G.-J. 2020. Early-
565 warning signals for marine anoxic events. *Geophysical Research Letters*, **47**, 1-9.
566 doi.org/10.1029/2020GL089183

568 Hiscott, R.N., Aksu, A.E., Mudie, P.J., Marret, F., Abrajano, T., Kaminski, M.A., Evans, J., Çakiroğlu, A.İ., Yaşar, D.
569 2007. A gradual drowning of the southwestern Black Sea shelf: Evidence for a progressive rather than abrupt

570 Holocene reconnection with the eastern Mediterranean Sea through the Marmara Sea Gateway. *Quaternary*
571 *International*, **167–168**, 19-34. doi.org/10.1016/j.quaint.2006.11.007
572
573 Hopmans, E.C., Weijers, J.W.H., Schefuß, E., Herfort, L., Sinninghe Damsté, J.S and Schouten, S. 2004. A novel
574 proxy for terrestrial organic matter in sediments based on branched and isoprenoid tetraether lipids. *Earth and*
575 *Planetary Science Letters*, **224**, 107-116. doi.org/10.1016/j.epsl.2004.05.012
576
577 Hopmans, E.C., Smit, N.T., Schwartz-Narbonne, R., Sinninghe Damste, J.S and Rush, D. 2021. Analysis of non-
578 derivatized bacteriohopanepolyols using UHPLC-HRMS reveals great structural diversity in environmental lipid
579 assemblages. *Organic Geochemistry*, **160**, 1-17. doi.org/10.1016/j.orggeochem.2021.104285
580
581 Huang, Y., Zheng, Y., Heng, P., Giosan, L and Coolen, M.J.L. 2021. Black Sea paleosalinity evolution since the last
582 deglaciation reconstructed from alkenone-inferred Isochrysidales diversity. *Earth and Planetary Science Letters*,
583 **564**, 1-9. doi.org/10.1016/j.epsl.2021.116881
584
585 Ion, G., Briceag, A., Vasiliu, D., Lupaşcu, N and Melinte-Dobrinescu, M. 2022. A multiproxy reconstruction of the
586 Late Pleistocene-Holocene paleoenvironment: New insights from the NW Black Sea. *Marine Geology*, **443**, 1-19.
587 doi.org/10.1016/j.margeo.2021.106648
588
589 Ivanova, E.V., Murdmaa, I.O., Chepalyga, A.L., Cronin, T.M., Pasechnik, I.V., Levchenko, O.V., Howe, S.S.,
590 Manushkina, A.V and Platonova, E.A. 2007. Holocene sea-level oscillations and environmental changes on the
591 Eastern Black Sea shelf. *Palaeogeography, Palaeoclimatology, Palaeoecology*, **246**, 228-259.
592 doi.org/10.1016/j.palaeo.2006.09.014
593
594 Ivanova, E.V., Marret, F., Zenina, M.A., Murdmaa, I.O., Chepalyga, A.L., Bradley, L.R., Schornikov, E.I., Levchenko,
595 O.V and Zyryanova, M.I. 2015. The Holocene Black Sea reconnection to the Mediterranean Sea: New insights
596 from the northeastern Caucasian shelf. *Palaeogeography, Palaeoclimatology, Palaeoecology*, **427**, 41-61.
597 doi.org/10.1016/j.palaeo.2015.03.027
598
599 Jaeschke, A., Hopmans, E. C., Wakeham, S. G., Schouten, S and Sinninghe Damsté, J.S. 2007. The presence of
600 ladderane lipids in the oxygen minimum zone of the Arabian Sea indicates nitrogen loss through anammox.
601 *Limnology and Oceanography*, **52**, 780–786. doi.org/10.4319/lo.2007.52.2.0780
602
603 Jensen, M.M., Kuypers, M.M.M., Lavik, G and Thamdrup, B. 2008. Rates and regulation of anaerobic ammonium
604 oxidation and denitrification in the Black Sea. *Limnology and Oceanography*, **53**, 23-36.
605 doi.org/10.4319/lo.2008.53.1.0023
606

607 Jones, G.A and Gagnon, A.R. 1994. Radiocarbon chronology of Black Sea sediments. *Deep-Sea Research 1*, **41**,
608 531-557. doi.org/10.1016/0967-0637(94)90094-9

610 Kalvelage, T., Lavik, G., Lam, P., Contreras, S., Arteaga, L., Löscher, C.R., Oschlies, A., Paulmier, A., Stramma, L
611 and Kuypers, M.M.M. 2013. Nitrogen cycling driven by organic matter export in the South Pacific oxygen
612 minimum zone. *Nature Geoscience*, **6**, 228-234. doi.org/10.1038/ngeo1739

614 Karner, M. B., DeLong, E. F., Karl, D. M. 2001. Archaeal dominance in the mesopelagic zone of the Pacific Ocean.
615 *Nature*, **409**, 507–510. doi.org/10.1038/35054051

617 Keeling, R.F., Körtzinger, A and Gruber, N. 2010. Ocean Deoxygenation in a Warming World. *Annual Review of*
618 *Marine Science*, **2**, 199-229. doi.org/10.1146/annurev.marine.010908.163855.

620 Knowles, R. 1982. Denitrification. *Microbiological Reviews*, **46**, 43-70. doi.org/10.1128/mr.46.1.43-70.1982.

622 Könneke, M., Bernhard, A.E., de la Torre, J.R., Walker, C.B., Waterbury, J.B and Stahl, D.A. 2005. Isolation of an
623 autotrophic ammonia-oxidizing marine archaeon. *Nature*, **437**, 543–546. doi.org/10.1038/nature03911

625 Koopmans, M.P., Köster, J., Van Kaam-Peters, H.M.E., Kenig, F., Schouten, S., Hartgers, W.A., de Leeuw, J.W and
626 Sinninghe Damsté, J.S. 1996. Diagenetic and catagenetic products of isorenieratene: Molecular indicators for
627 photic zone anoxia. *Geochimica et Cosmochimica Acta*, **60**, 4467-4496. doi.org/10.1016/S0146-6380(97)00025-
628 9

630 Kuenen, J.G and Robertson, L.A. 1988. Ecology of nitrification and denitrification. *In:* Cole, J.A and Ferguson, S.J
631 (eds.), The Nitrogen and Sulphur Cycles. Cambridge University Press, Cambridge, pp. 161-218.

633 Kusch, S., Wakeham, S.G and Sepúlveda, J. 2022. Bacteriohopanepolyols across the Black Sea redoxcline trace
634 diverse bacterial metabolisms. *Organic Geochemistry*, **172**, 1-18. doi.org/10.1016/j.orggeochem.2022.104462

636 Kuypers, M.M.M., Sliekers, A.O., Lavik, G., Schmid, M., Barker Jørgensen, B., Kuenen, J.G., Sinninghe Damsté,
637 J.S., Strous, M and Jetten, M.S.M. 2003. Anaerobic ammonium oxidation by anammox bacteria in the Black Sea.
638 Nature, 422, 608-611. doi.org/10.1038/nature01472

640 Kwiecien, O., Arz, H.W., Lamy, F., Wulf, S., Bahr, A., Röhl, U and Haug, G.H. 2008. Estimated Reservoir Ages of
641 the Black Sea Since the Last Glacial. *Radiocarbon*, 50, 99-118. doi.org/10.1017/S0033822200043393

643 Lam, P., Jensen, M.M., Lavik, G., McGinnis, D.F., Müller, B., Schubert, C.J., Amann, R., Thamdrup, B., and Kuypers,
644 M.M.M. 2007. Linking crenarchaeal and bacterial nitrification to anammox in the Black Sea. *PNAS*, **104**, 7104-
645 7109. doi.org/10.1073/pnas.061108110

647 Limaye, R.B., Padmalal, D and Kumaran, K.P.N. 2017. Cyanobacteria and testate amoeba as potential proxies for
648 Holocene hydrological changes and climate variability: Evidence from tropical coastal lowlands of SW India.
649 *Quaternary International*, **443**, 99-114. doi.org/10.1016/j.quaint.2016.09.044

651 Major, C., Ryan, W., Lericolais, G and Hajdas, I. 2002. Constraints on Black Sea outflow to the Sea of Marmara
652 during the last glacial–interglacial transition. Marine Geology, 190, 19-34. doi.org/10.1016/S0025-
653 3227(02)00340-7

655 Major, C., Goldstein, S., Ryan, W., Lericolais, G., Piotrowski, A.M and Hajdas, I. 2006. The co-evolution of Black
656 Sea level and composition through the last deglaciation and its paleoclimatic significance. *Quaternary Science*
657 *Reviews*, **25**, 2031-2047. doi.org/10.1016/j.quascirev.2006.01.032

659 Marret, F., Mudie, P., Aksu, A and Hiscott, R.N. 2009. A Holocene dinocyst record of a two-step transformation
660 of the Neoeuxinian brackish water lake into the Black Sea. *Quaternary International*, **197**, 72-86.
661 doi.org/10.1016/j.quaint.2007.01.010

663 McCarthy, J.J., Yilmaz, A., Coban-Yildiz, Y and Nevins, J.L. 2007. Nitrogen cycling in the offshore waters of the
664 Black Sea. Estuarine, Coastal and Shelf Science. 74, 493-514.

666 Ménot, G and Bard, E. 2012. A precise search for drastic temperature shifts of the past 40,000 years in
667 southeastern Europe. *Palaeoceanography*, **27**, 1-13. doi.org/10.1029/2012PA002291

669 Mertens, K.N., Bradley, L.R., Takano, Y., Mudie, P.R., Marret, F., Aksu, A.E., Hiscott, R.N., Verleye, T.J., Mousing,
670 E.A., Smyrnova, L.L., Bagheri, S., Mansor, M., Pospelova, V and Matsuoka, K. 2012. Quantitative estimation of
671 Holocene surface salinity variation in the Black Sea using dinoflagellate cyst process length. *Quaternary Science*
672 *Reviews*, **39**, 45-59. doi.org/10.1016/j.quascirev.2012.01.026

674 Murray, J.W., Jannasch, H. W., Honjo, S., Anderson, R. F., Reeburgh, W. S., Top, Z., Friederich, G. E., Codispoti, L.
675 A and Izdar, E. 1989. Unexpected changes in the oxic/anoxic interface in the Black Sea. *Nature*, **337**, 411-413.
676 doi.org/10.1038/338411a0

678 Murray, J.W., Codispoti, L.A and Friederich, G.E. 1995. Oxidation-reduction environments: the suboxic zone in
679 the Black Sea. *In:* Huang C.P., O'Melia C.R., Morgan J.J. (Eds) Aquatic Chemistry: Interfacial and Interspecies
680 Processes. ACS Advances in Chemistry Series. No. 224. pp. 157-176. doi.org/10.1021/ba-1995-0244.ch007

681

682   Naafs, B.D.A., Monteiro, F.M., Pearson, A., Higgins, M.B., Pancost, R.D and Ridgwell, A. 2019. Fundamentally

683   different global marine nitrogen cycling in response to severe ocean deoxygenation. *Proceedings of the National*

684   *Academy of Sciences*, **116**, 24979-24984. doi.org/10.1073/pnas.1905553116

685

686   Nicholas, W.A., Chivas, A.R., Murray-Wallace, C.V and Fink, D. 2011. Prompt transgression and gradual

687   salinisation of the Black Sea during the early Holocene constrained by amino acid racemization and radiocarbon

688   dating. *Quaternary Science Reviews*, **30**, 3769-3790. doi.org/10.1016/j.quascirev.2011.09.018

689

690   Özsoy, E and Ünlüata, Ü. 1997. Oceanography of the Black Sea: A review of some recent results. *Earth Science*

691   *Reviews*, **42**, 231-272. doi.org/10.1016/S0012-8252(97)81859-4

692

693   Pérez Gallego, R., von Meijenfeldt, B., Bale, N.J., Sinninghe Damsté, J.S and Villanueva, L. 2025. Emergence and

694   evolution of heterocyte glycolipid biosynthesis enabled specialized nitrogen fixation in cyanobacteria.

695   Microbiology, 122. doi.org/10.1073/pnas.2413972122.

696

697   Piper, D.Z and Calvert, S.E. 2011. Holocene and late glacial palaeoceanography and palaeolimnology of the Black

698   Sea: Changing sediment provenance and basin hydrography over the past 20,000 years. *Geochimica et*

699   *Cosmochimica Acta*, **75**, 5597-5624. doi.org/10.1016/j.gca.2011.07.016

700

701   Ploug, H. 2008. Cyanobacterial surface blooms formed by Aphanizomenon sp. and Nodularia spumigena in the

702   Baltic Sea: Small-scale fluxes, pH, and oxygen microenvironments. *Limnology & Oceanography*, **53**, 914-921.

703   doi.org/10.4319/lo.2008.53.3.0914

704

705   Reimer, P.J., Austin, W.E.N., Bard, E., Bayliss, A., Blackwell, P.G., Bronk Ramsey, C., Butzin, M., Cheng, H.,

706   Edwards, R.L., Friedrich, N., Grootes, P.M., Guilderson, T.P., Hajdas, I., Heaton, T.J., Hogg, A.G., Hughen, K.A.,

707   Kromer, B., Manning, S.W., Muscheler, R., Palmer, J.G., Pearson, C., van der Plicht, J., Reimer, R.W., Richards,

708   D.A., Scott, E.M., Southon, J.R., Turney, C.S.M., Wacker, L., Adolphi, F., Büntgen, U., Capano, M., Fahrni, S.M.,

709   Fogtmann-Schulz, A., Friedrich, R., Köhler, P., Kudsk, S., Miyake, F., Olsen, J., Reinig, F., Sakamoto, M., Sookdeo,

710   A and Talamo, S. 2020. The IntCal20 Northern Hemisphere Radiocarbon Age Calibration Curve (0–55 cal kBP).

711   *Radiocarbon*, **62**, 725–757. doi.org/10.1017/RDC.2020.41

712

713   Rush, D., Sinninghe Damsté, J.S., Poulton, S.W., Thamdrup, B., Garside, A.L., Acuña González, J., Schouten, S.,

714   Jetten, M.S.M and Talbot, H.M. 2014. Anaerobic ammonium-oxidising bacteria: A biological source of the

715   bacteriohopanetetrol stereoisomer in marine sediments. *Geochimica et Cosmochimica Acta*, **140**, 50-64.

716   doi.org/10.1016/j.gca.2014.05.014

717

718   Rush, D and Sinninghe Damsté, J.S. 2017. Lipids as paleomarkers to constrain the marine nitrogen cycle.
719   *Environmental Microbiology*, **19**, 2119-2132. doi.org/10.1111/1462-2920.13682

720

721   Schouten, S., Hopmans, E.C and Sinninghe Damsté, J.S. 2013. The organic geochemistry of glycerol dialkyl
722   glycerol tetraether lipids: A review. *Organic Geochemistry*, **54**, 19-61.
723   doi.org/10.1016/j.orggeochem.2012.09.006

724

725   Schrader, H.-J. 1979. Quaternary Paleoclimatology of the Black Sea basin. *Sedimentary Geology*, **23**, 165-180.
726   doi.org/10.1016/0037-0738(79)90013-7

727

728   Schwartz-Narbonne, N., Schaeffer, P., Hopmans, E.C., Schenesse, M., Charlton, E.A., Jones, D.M., Sinninghe
729   Damsté, J.S., Farhan, M., Haque, U., Jetten, M.S.M., Lengger, S.K., Murrell, J.C., Normand, P., Nuijten, G.H.L.,
730   Talbot, H.M and Rush, D. 2020. A unique bacteriohopanetetrol stereoisomer of marine anammox. *Organic
731   Geochemistry*, **143**, 1-10. doi.org/10.1016/j.orggeochem.2020.103994

732

733   Shumilovskikh, L.S., Tarasov, P., Arz, H.W., Fleitmann, D., Marret, F., Nowaczyk, N., Plessen, B., Schlütz, F and
734   Behling, H., 2012. Vegetation and environmental dynamics in the southern Black Sea region since 18 kyr BP
735   derived from the marine core 22-GC3. *Palaeogeography, Palaeoclimatology, Palaeoecology*, **337–338**, 177-193.
736   doi.org/10.1016/j.palaeo.2012.04.015

737

738   Sinninghe Damste, J.S., Wakeham, S.G., Kohnen, M.E.L., Hayes, J.M., de Leeuw, J.W. 1993. A 6,000–year
739   sedimentary molecular record of chemocline excursions in the Black Sea. *Nature*, **362**, 827–829.
740   doi.org/10.1038/362827a0

741

742   Sinninghe Damsté, J.S., Schouten, S., Hopmans, E.C., van Duin, A.C.T and Geenevasen, A.J.A. 2002. Crenarchaeol.
743   *Journal of Lipid Research*, **43**, 1641-1651.

744

745   Sollai, M., Hopmans, E.C., Bale, N.J., Mets, A., Warden, L., Moros, M and Sinninghe Damsté, J.S. 2017. The
746   Holocene sedimentary record of cyanobacterial glycolipids in the Baltic Sea: an evaluation of their application
747   as tracers of past nitrogen fixation. *Biogeosciences*, **14**, 5789–5804. doi.org/10.5194/bg-14-5789-2017

748

749   Soulet, G., Ménot, G., Lericolais, G and Bard, E. 2011. A revised calendar age for the last reconnection of the
750   Black Sea to the global ocean. *Quaternary Science Reviews*, **30**, 1019-1026.
751   doi.org/10.1016/j.quascirev.2011.03.001

752

753   Stuiver, M and Polach, H.A. 1977. Discussion Reporting of 14C Data. *Radiocarbon*, **19**, 35-363. doi.org/
754   10.1017/S0033822200003672

755

756 van de Graaf, A.A., de Bruijn, P., Robertson, L.A., Jetten, M.S.M and Kuenen, J.G. 1997. Metabolic pathway of
757 anaerobic ammonium oxidation on the basis of 15N studies in a fluidized bed reactor. *Microbiology*, **143**, 2415–
758 2421. doi.org/10.1099/00221287-143-7-2415

760 van der Meer, M.J.M., Sangiorgi, F., Baas, M., Brinkhuis, H., Sinninghe Damsté, J.S and Schouten, S. 2008.
761 Molecular isotopic and dinoflagellate evidence for Late Holocene freshening of the Black Sea. *Earth and*
762 *Planetary Science Letters*, **267**, 426-434. doi.org/10.1016/j.epsl.2007.12.001

764 van Kemenade, Z.R., Cutmore, A., Hennekam, R., Hopmans, E.C., van der Meer, M.T.J., Mojtahid, M., Jorissen,
765 F.J., Bale, N.J., Reichart, G.-J., Sinninghe Damsté, J.S and Rush, D. 2023. Marine nitrogen cycling dynamics under
766 altering redox conditions: insights from deposition of sapropels S1 and the ambiguous S2 in the Eastern
767 Mediterranean Sea. *Geochimica et Cosmochimica Acta*, **354**. doi.org/10.1016/j.gca.2023.06.018

769 Verleye, T.J., Mertens, K.N., Louwye, S and Arz, H.W. 2009. Holocene salinity changes in the southwestern black
770 sea: A reconstruction based on dinoflagellate cysts. *Palynology*, **33**, 77-100.

772 Villareal, T.A. 1992. Marine Nitrogen-Fixing Diatom-Cyanobacteria Symbioses. *In:* Carpenter, E.J., Capone, D.G
773 and Rueter, J. G (eds.), Marine Pelagic Cyanobacteria: Trichodesmium and other Diazotrophs.
774 Springer:Dordrecht, pp. 163-175.

776 Wegwerth, A., Eckert, S., Dellwig, O., Schnetger, B., Severmann, S., Weyer, S., Brüske, A., Kaiser, J., Köster, J.,
777 Arz, H.W and Brumsack, H.-J. 2018. Redox evolution during Eemian and Holocene sapropel formation in the
778 Black Sea. *Palaeogeography, Palaeoclimatology, Palaeoecology*, **489**, 249-260.

780 Whitton, B.A and Mateo, P. 2012. Rivulariaceae. In: Whitton, B.A (ed.), Ecology of Cyanobacteria II.
781 Springer:Dordrecht, pp. 561–591. doi.org/10.1007/978-94-007-3855-3_22

783 Wörmer, L., Cires, S., Velazquez, D., Quesada, A and Hinrichs, K.-U. 2012. Cyanobacterial heterocyst glycolipids
784 in cultures and environmental samples: Diversity and biomarker potential. *Limnology & Oceanography*, **57**,
785 1775-1788. doi.org/10.4319/lo.2012.57.6.1775

787 Wuchter, C., Abbas, B., Coolen, M.J.L., Herfort, L., van Bleijswijk, J., Timmers, P., Strous, M., Teira, E., Herndl,
788 G.J., Middelburg, J.J., Schouten, S and Sinninghe Damsté, J.S. 2006. Archaeal nitrification in the ocean. *PNAS*,
789 **103**, 12317-12322. doi.org/10.1073/pnas.0600756103
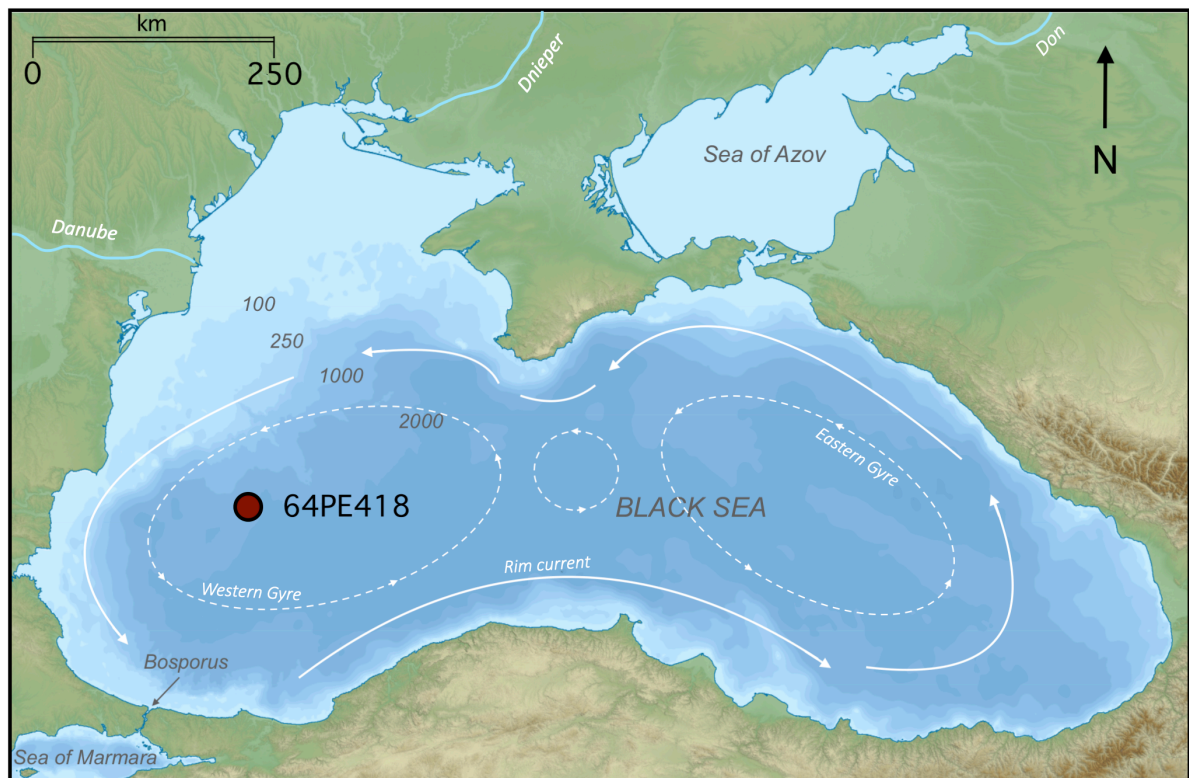
793
794 **Figure 1:** Map of the Black Sea basin, showing the major surface circulation, depth contours (mbsl) and location
795 of core 64PE418. (Adapted from: Giorgi Balakhadze, English Wikipedia, 2016).

796
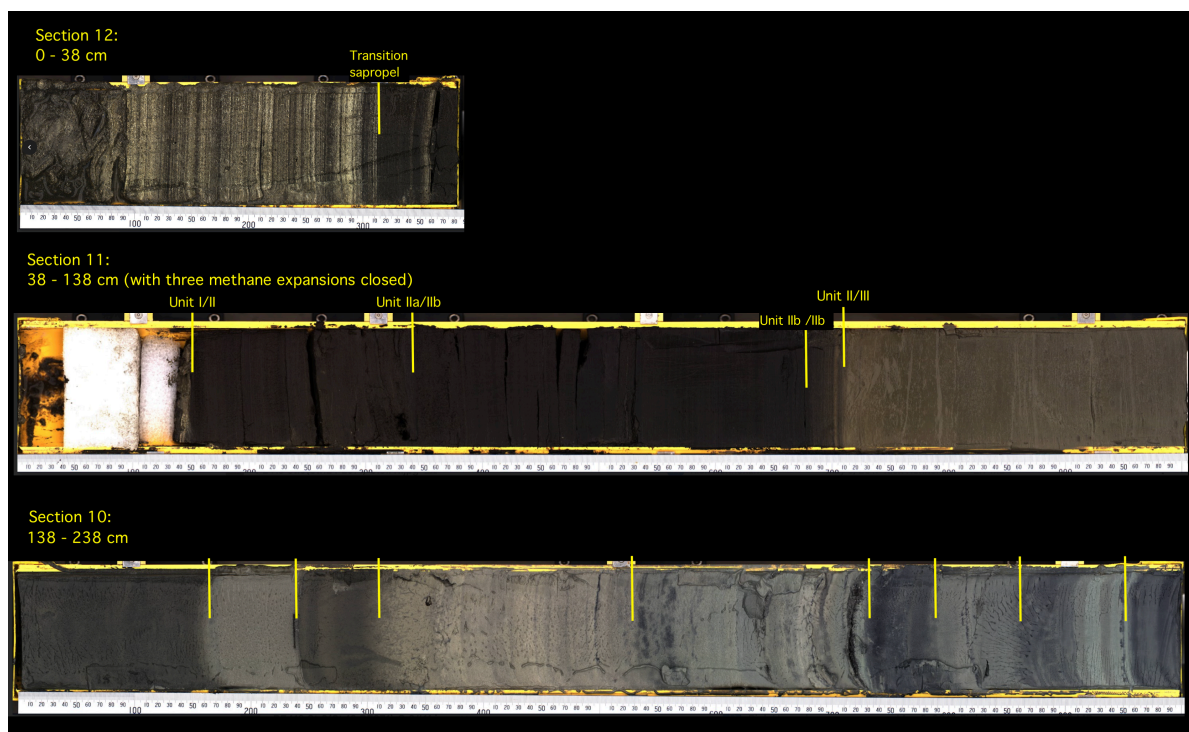
797
798 **Figure 2:** Scan of core 64PE418 showing colour changes and the depth of unit boundaries. Unit boundaries are
799 defined according to Arthur & Dean (1998) and have been identified by colour changes and XRF-core-scan
800 changes in Ti and Ca (Fig. S1).

801
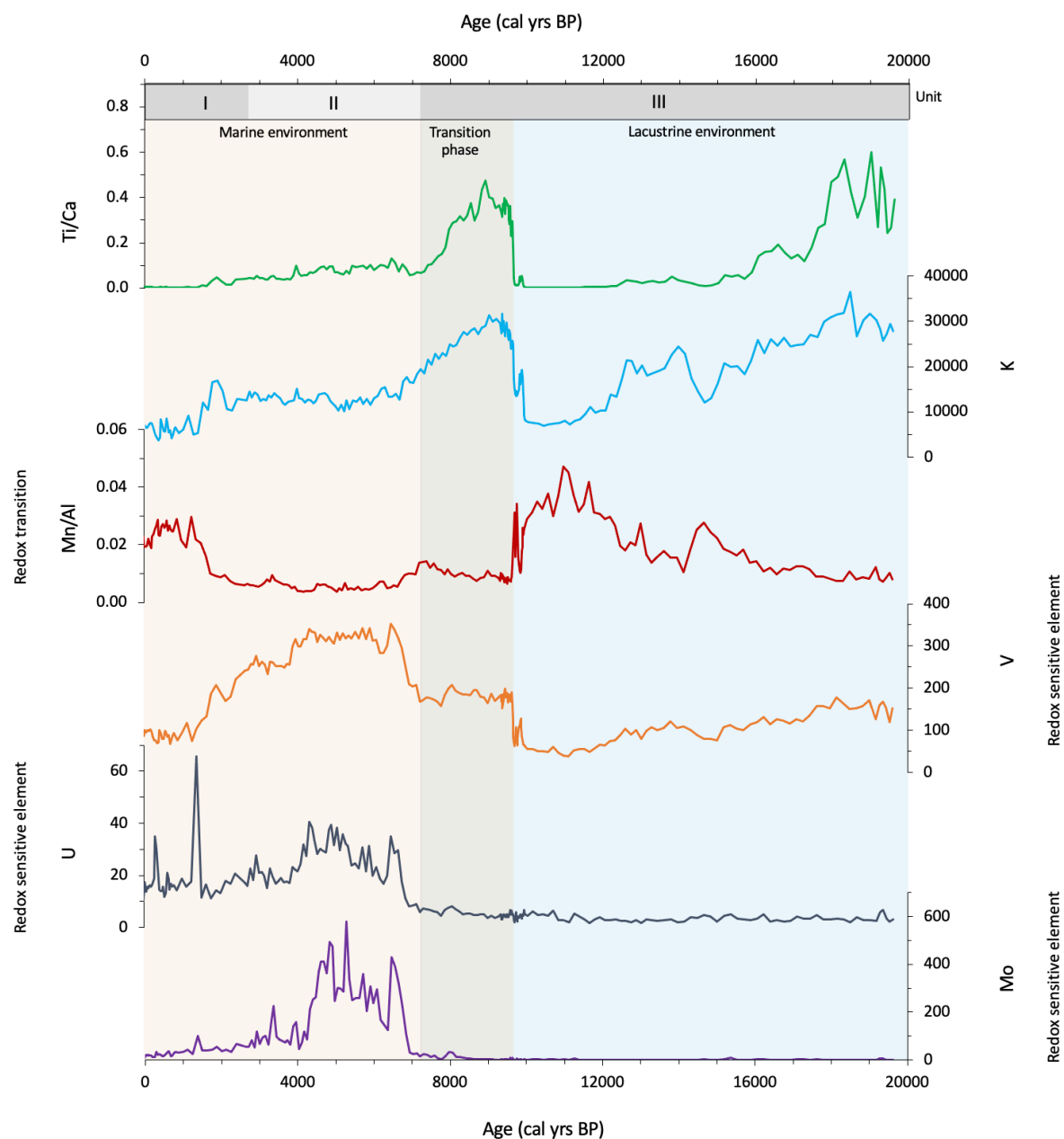
Figure 3: Changes over the last 19.6 ka in the elemental content of core 64PE418, as measured through

803 calibrated XRF-core-scanning (ppm) using the methods described in Hennekam et al. (2020).

804
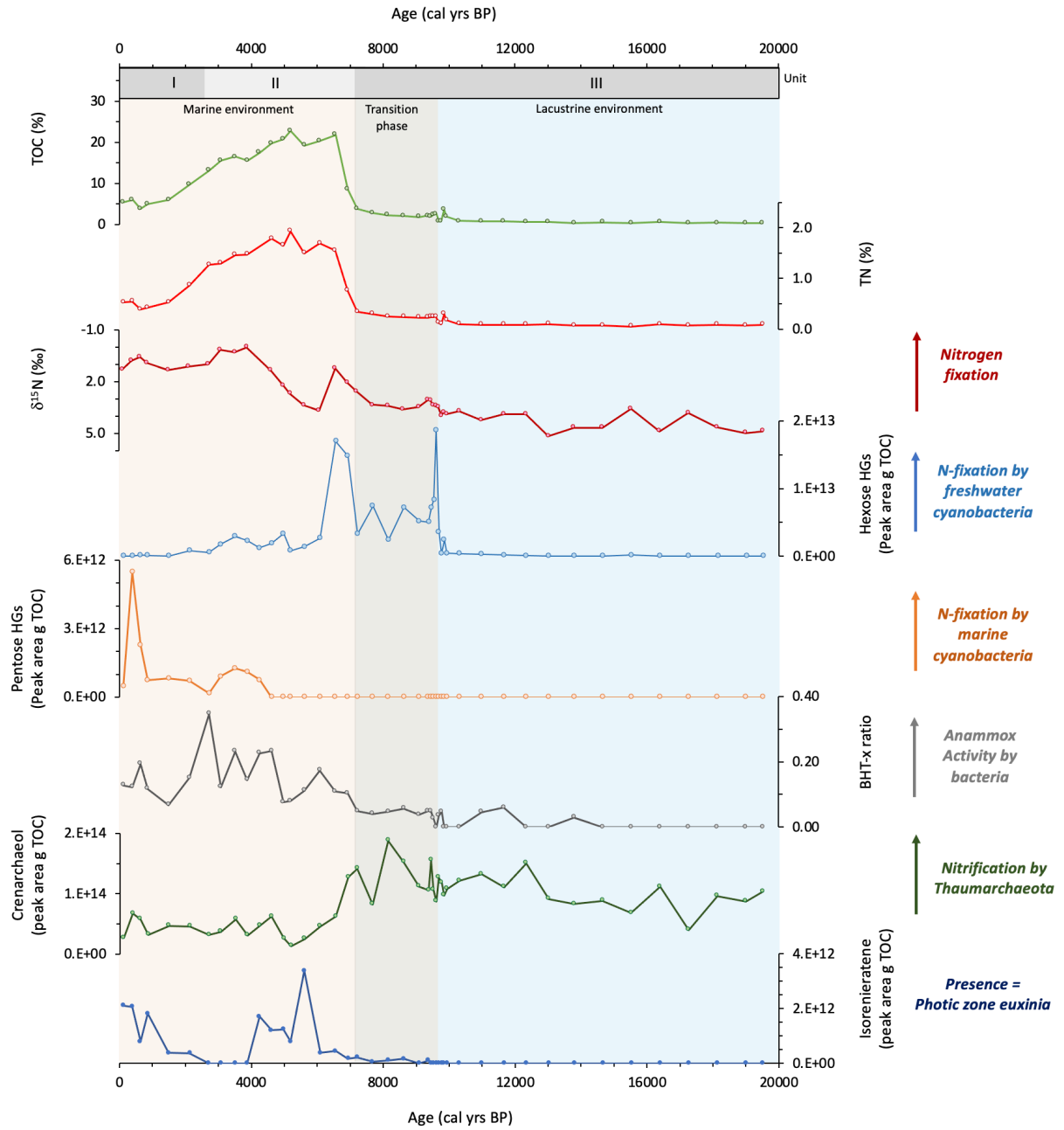
Figure 4: Geochemical records from Black Sea core 64PE418 of: a) TOC (%); b) TN (%); c) $\delta^{15}N_{bulk}$ (‰); d) hexose HGs (peak area per g TOC); e) pentose HGs (peak area per g TOC); f) BHT-x ratio; g) crenarchaeol (peak area per g TOC); h) isorenieratene (peak area per g TOC).
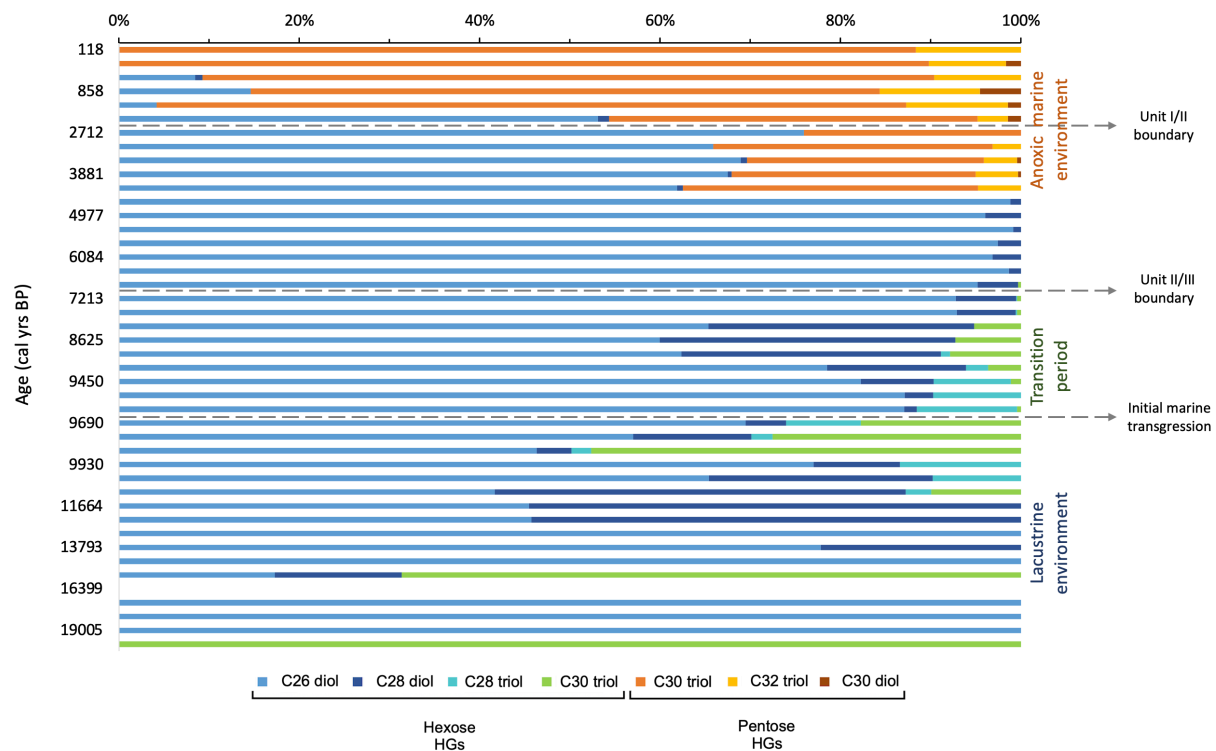
Figure 5: Changes over time in relative abundance of hexose and pentose HGs present in Black Sea core 64PE418